Life Cycle Assessment of Low-Dimensional Materials for Perovskite Photovoltaic Cells

Achyuth Ravilla[1], Carlo A.R. Perini[2], Juan-Pablo Correa-Baena[2], Anita W.Y. Ho-Baillie[3], Ilke Celik[1*]

[1] Department of Civil and Environmental Engineering, Portland State University, Portland, 97201, OR, USA.
[2] School of Material Science and Engineering, Georgia Institute of Technology, Atlanta, 30332, GA, USA.
[3] School of Physics and University of Sydney Nano Institute, The University of Sydney, Sydney, NSW 2006, Australia.
*Corresponding author, Department of Mechanical and Material Engineering, Portland State University, Portland, 97201, OR, USA.
E-mail address: ilke@pdx.edu (Ilke Celik).

Abstract:

While perovskite solar cells (PSC) have a high potential of achieving commercial-scale manufacturing, they still face some deficiencies regarding rapid degradation in the presence of moisture, oxygen, and high-temperature exposure. To address these challenges, recent research has identified lower dimensional (LD) materials as promising candidates to improve the stability and power conversion efficiency (PCE) of PCSs. The goal of this study is to analyze the environmental performance of LD material-based PSCs (*ld*-PSC) through a comprehensive life cycle assessment, comparing their environmental performance with reference PSC and commercial photovoltaics (PV) technologies including single-crystalline (c-Si), copper indium gallium diselenide (CIGS) and cadmium telluride (CdTe). To achieve this objective, we evaluated five LD materials such as graphene, reduced graphene oxide (rGO), graphene quantum dots (GQDs), molybdenum disulfide (MoS_2), and black phosphorus (BP) that are commonly studied in experimental works, and two distinct *ld*-PSC configurations such as Alt-1 and Alt-2, featuring LD materials with lower environmental and comparatively higher among those studied. A comparison of LD materials on a unit mass basis reveals that rGO, graphene, and MoS_2 are the most environmentally friendly options. However, their environmental impact changes significantly when incorporated into *ld*-PSC configurations based on the type and amount of chemicals used for the dispersion which emphasizes the importance of carefully selecting the chemicals used for dispersion. Our results show that the Alt-1 configuration is ~25% lower and the Alt-2 configuration has ~ 15% higher average environmental impacts compared to reference PSCs. Further analyses show that at 20% benchmark PCE, *ld*-PSC has the potential to outperform the environmental performance of all conventional technologies, even with a lifetime up to 2.5 times shorter. Additionally, *ld*-PSC has a lower energy payback period compared to commercial PV technologies. These findings demonstrate the significant potential of *ld*-PSC for the commercial application of PSC technology.

1. Introduction

Globally, solar power installations have surged to a remarkable 1.2 TW_{dc}, with the United States contributing significantly by reaching 142 GWdc installations[1,2]. At present, around 5% of global electricity is generated from solar photovoltaics (PV), and it is expected to make up a significantly higher percentage of global electricity production by the year 2050, with 38% [3,4]. To achieve this goal, large-scale deployment of durable and efficient solar technologies is required. Currently, >90% of the global PV market is dominated by crystalline silicon solar PVs[5,6]. Among the crystalline silicon PV technologies, the single-crystalline (c-Si) PV technology has reached the highest power conversion efficiency (PCE) rate, 26.1%[7]. There have been significant efforts in recent years to reduce the materials and energy utilization in c-Si synthesis[8], yet, the processing of the c-Si PV is still expensive and less environmentally friendly compared to thin film PV technologies[9,10]. Among emerging thin-film PV technologies, perovskite solar cells (PSCs) have been recognized as one of the most promising PV technologies with the potential to be a low-cost and environmentally friendly alternative to the c-Si PVs[9,11–13].

The attention on PSCs over other PV technologies is driven by the favorable combination of high performances, ease of processing, and tunable optical properties offered by the perovskite active layer[12–14]. Such properties make PSCs particularly promising both in single- and multi-junction applications, enabling lower costs and higher energy yields than existing PV technologies[12–19]. The best-recorded PCE of single junction PSCs has reached 26.1%, which is equivalent to c-Si PV and perovskite-Si tandem devices have even surpassed 30% PCE[7]. Despite their great potential, PSCs are still limited by poor stability[20–22]. The active layer degrades in the presence of moisture, oxygen, high temperature, or upon reactions with other layers in the stack[14,23]. Halide ions in the perovskite film can react with interlayers and with the metal electrodes, leading to a rapid performance loss [6,23–25]. Previous studies have suggested several approaches to enhance stability and prevent the degradation of PSCs. These include the use of various thin film encapsulation materials, the choice of charge transport layers with large ionization energy and high crystallization temperature, material composition tuning such as converting three-dimensional (3D) perovskite to two-dimensional (2D) perovskite, the passivation of grain boundaries with hydrophobic coatings, and the incorporation of lower dimensional material (LD) materials into PSC structure[23,25–31]. Among these approaches, LD material integration has emerged as a promising strategy and an extensively investigated approach in recent studies [6,22,32–34].

LD materials including graphene-related materials (graphene, reduced graphene oxide (rGO), and graphene quantum dots (GQDs)), black phosphorus (BP), and transition metal dichalcogenides such as molybdenum disulfide (MoS_2), tungsten disulfide (WS_2), and tungsten diselenide (Wse_2) have been identified as promising candidates to improve the thermal and chemical stability of PSCs [6,20,22,33–37]. Incorporating LD materials in different layers of PSCs (e.g., electrode, charge transport layers, or as additives to the absorber layer), works as a good barrier for moisture and oxygen, restrains the migration of ions (from the perovskite into the metal electrode and vice versa), and improves thermal stability[6,37]. As such, LD materials have succeeded in increasing the stability of PSCs [33,37]. LD materials can also enhance the PCE of PSCs with their high carrier mobilities, tunable work function, transparency, and mechanical flexibility[22,33,37]. In addition, carbon-based materials have been investigated as potential alternatives for both front contact as a replacement for transparent conductive oxides and back contact (BC) for metal electrode

replacement[6,37–39]. Graphene-based substrates were identified as excellent candidates for replacing the environmentally harmful indium in the fabrication of transparent conductive oxide-free flexible PSCs, making them most suitable for building integrated PV applications[6,22,38,40–42]. Utilizing carbon based electrodes used as the BC helps in developing hole transport layer (HTL) free and metal-free PSCs, paving the way for cost-effective, hydrophobic, thermally stable, highly efficient, and environmentally friendly PSC devices for future energy generation[6,11,21,22,39].

While the research and development on enhancing the PCE and stability of PSC technology using LD material continues, it is also essential to identify the environmental impacts associated with PSC in the early stage of this technology's development. After conducting a comprehensive literature review, we have identified that assessments on environmental impacts, and commonly reported sustainability metrics (energy demand, payback time, etc.) of LD material-based PSCs *(ld*-PSC) are missing. Furthermore, there is a lack of comparative analysis between the environmental performance of *ld*-PSCs and commercial PV technologies.

In this study, we identify the critical materials and processes that influence the environmental sustainability of *ld*-PSC for large-scale manufacturing. This is the first study incorporating sustainability tools such as life cycle assessment (LCA) to provide the design and fabrication principles for the sustainable development of *ld*-PSC. First, we selected LD materials that are commonly incorporated into PSCs and have demonstrated significant enhancement in both stability and PCE. Subsequently, we identified the most scalable production methods for these LD materials for the integration of PSCs and provided life cycle inventories for large-scale production of *ld*-PSCs. Our study encompasses two distinct *ld*-PSC configurations: Alt-1, which incorporates LD materials with lower environmental impacts at each layer, and Alt-2, which employs LD materials with relatively higher environmental impacts for each layer integration. Then, we compared the environmental performance of these two alternative PSCs with that of reference PSCs without LD materials integration and commercial PV technologies including c-Si, copper indium gallium diselenide (CIGS), and cadmium telluride (CdTe). Following this comparative analysis, a sensitivity analysis was conducted to assess and compare the environmental performance of two alternative *ld*-PSC configurations with that of commercial PV technologies, considering a range of lifetime and PCE values. Additional analysis comparing the global warming potential (GWP) and energy payback time (EPBT) of these two alternative *ld*-PSC configurations with the reference PSC and established PV technologies is also included in the study.

2. Methods

2.1. Goal and scope

The goal of this study is to assess the environmental performance of *ld*-PSC in comparison to reference PSC and commercial PV technologies. The LCA was carried out in accordance with principles outlined in ISO 14040:2006[43] and ISO 14044:2006[44] guidelines. Additionally, we followed methodological guidelines provided by the International Energy Agency, which include recommendations for PV-specific technical aspects, life cycle inventory modeling, and life cycle impact assessment methods[45]. The results of this study will inform researchers and decision-makers in understanding the environmental performance of *ld*-PSC. Additionally, the findings from this study provide sustainable design principles for the commercialization of PSC technologies.

A cradle-to-end-of-use system boundary was selected, which includes raw material extraction, PSC manufacturing, and LD material deposition. We considered only electricity generation from *ld*-PSCs during operations phase and didn't consider maintenance required during operations. This *ld*-PSC technology is still at the research stage and considered relatively new, which introduces a higher level of uncertainty in assessing end-of-life phases. Therefore, we exclude end-of-life phase from our analysis. The functional unit chosen for this LCA analysis was 1 kWh of electricity generated by *ld*-PSC in their lifetime. For LCA analysis, GaBi ts 10.0[46] software was used, and impact assessment was carried out using the Tool for the Reduction and Assessment of Chemicals (TRACI) 2.1[47] method. The ten midpoint impact categories of TRACI impact assessment method: acidification (kg $SO_{2\text{-eq.}}$), ecotoxicity (CTU_e), eutrophication (kg N_{eq}), GWP (kg $CO_{2\text{-eq}}$), human toxicity (CTU_h), cancer and non-cancer, human health particular air (kg $PM_{2.5\text{-eq}}$), resources-fossil fuels (MJ $_{\text{surplus energy}}$), ozone depletion (kg $CFC11_{eq}$), and smog (kg $O_{3\text{-eq}}$) were modeled. In addition, this study calculated the cumulative energy demand (CED) and energy payback time (EPBT)[15] for all the assessed PV technologies.

2.2. Selection of LD materials and their manufacturing processes for PSC integration

The reported experimental studies that incorporate LD materials into PSCs provided the baseline secondary data for this LCA study[48–57]. The summary of improvements in PV device parameters after the incorporation of LD materials into each layer is also provided in Table S.6. Recent literature shows that LD materials are mainly used to improve the stability and PCE of materials in electron transporting layer (ETL), absorber, and hole transporting layer (HTL) of regular PSCs. The commonly employed materials in the layers of reference PSC consist of SnO_2 for ETL, $CH_3NH_3PbI_3$ for absorber, and Spiro-OMeTAD for HTL. Note that the utilization of spiro-OMeTAD in mass-scale production of PSC has concerns due to its high cost [11]. However, the current literature places significant emphasis on the integration of LD materials into this material [53,54,57] compared to low-cost HTL materials (see the SI for our additional analysis based on a low-cost HTL alternative using copper thiocyanate (CuSCN)). Furthermore, the inverted PSC structure with poly (3,4 ethylenedioxythiophene)-polystyrene sulfonate (PEDOT: PSS) as HTL and 6,6-phenylC61butyric acid methyl ester (PCBM) with LD materials integration[58] also assessed in SI.

The LD materials considered in this study were categorized into three groups: 1) Graphene-related materials (Graphene ink, rGO, and GQDs), 2) Transition metal dichalcogenide (MoS_2) 3) BP. Table 1 shows various LD materials that are incorporated into the PSC structure and their benefits over reference PSC. Previous literature shows that the incorporation of these LD materials into ETL, absorber, and HTL of PSC enhanced the PCE by more than 5% and retained >90% of the initial efficiencies when compared to the conventional PSC[48–54]. Despite the low cost and excellent mechanical stability, PSCs with carbon-based BC typically exhibit lower PCE values when compared to those utilizing metal back contacts [6,39]. As shown in Table 1, the incorporation of graphene as a BC for PSCs does not result in any enhancements in PCE when compared to the reference PSC using metal BC[39]. Similarly, the incorporation of graphene as a transparent conductive electrode did not yield any significant improvements in the PCE of *ld*-PSC [6,37,38]. Therefore, we focused our attention on integrating LD materials exclusively into the ETL, absorber, and HTL of PSC.

Table 1 Different LD materials integration into PSC structure and their benefits. Note: In some of the studies where LD materials were integrated into absorber and HTL of PSC structures, TiO_2 was used as ETL instead of SnO_2. These studies were still included in our analysis because the observed enhancements in the PCE and stability in this ld-PSC were primarily attributed to improvements in the absorber layer and HTL rather than the ETL.

PSC Layer	LD Material Integration	Reported Properties	Reference
ETL	Graphene	15% increase in PCE and retaining 90% initial PCE values	48
	GQDs	24% increase in PCE and retaining 95% of initial PCE values	49
	BPQDs	15% increase in PCE and retaining 90% of initial PCE values	55
Absorber layer	BP-nano	10% increase in PCE and retaining 94% of initial PCE values	56
	rGO	30% increase in PCE and retaining 90% of initial PCE values	51
	GQDs	10% increase in PCE and retaining 94% of initial PCE values	52
HTL	BP-nano	25% increase in PCE and retaining 90% of initial PCE values	53
	MoS_2	10% increase in PCE and retaining 75% of initial PCE values	54
	rGO	5% increase in PCE and retaining 75% of initial PCE values	57
BC	Graphene	Negligible improvements in PCE and retained 95% of its initial PCE values	39

Fig.1 shows the integration of LD materials into PSC's layers and possible manufacturing techniques for these LD materials. We went through a rigorous elimination process to identify the most scalable methods that can be used for the incorporation of LD materials with PV systems. We eliminated the processes that are energy and time intensive, and not cost effective. For example, graphene-related materials can be produced by exfoliation and chemical oxidation-reduction of graphite, and chemical vapor deposition methods. Among these production routes, exfoliation and chemical oxidation-reduction of graphite methods are most suited for commercial-scale production[59–61]. This is because chemical vapor deposition is an energy-intensive and expensive method[61]. Among exfoliation-based graphene synthesis routes, we chose electrochemical exfoliation using potassium hydroxide over the liquid exfoliation method because it yields high quality graphene sheets without using toxic solvents and is a simple process for commercial production[60,61]. Other graphene-related compounds, such as rGO and GQDs, are derived from graphene oxide (GO), which is produced by the chemical oxidation of graphite[62]. The chemical oxidation of graphite can be achieved by the modified hummers (Bangal variant) process [62]. The scalable production of GQDs from GO can be obtained using chemical oxidation and hydrothermal methods[63]. We chose the continuous hydrothermal approach developed by Kellici et al for commercial-scale GQD manufacture since it is a rapid method and suitable for large-scale production[63,64]. For rGO synthesis, among chemical and thermal reduction methods, we chose the former because it is a cost-effective method for producing rGO on a large scale[61]. Among various synthesis routes for MoS_2 nanosheets, we chose the solvothermal method as a

feasible solution for large-scale production[65]. The solvothermal method for generating MoS_2 nanosheets is a low-temperature and one-step technique[65]. We found common methodologies for the production of BP-nano and black phosphorus quantum dots (BPQDs), such as electrochemical exfoliation and liquid phase exfoliation[50,66]. Because of its low cost and simple operational procedures, we chose liquid phase exfoliation as the most scalable approach for BP-nano and BPQDs[66].

2.3. Life cycle inventories

The life cycle inventories were created using most recent data for mass-scaled PV production and experimental data for LD specific components. First, the materials and energy inventories for PSC, c-Si, CIGS, and CdTe modules were developed using the IEA-Photovoltaic Power Systems (PVPS) TASK 12 report[45] as a baseline for manufacturing of a 1 m^2 PV panel. For *ld*-PSC configuration, the life cycle inventories were prepared by separately analyzing PSC production and LD material deposition. The synthesis of the PSC component involved sputtering the ETL onto FTO/glass, with subsequent deposition of the absorber layer and HTL deposited by slot die coating [67,68]. The metal electrode was then deposited using the evaporation method [67]. These studies were selected because they addressed deposition techniques that are suitable for large-scale production. Further, the inventories for incorporating LD materials into 1 m^2 of PSC were created based on literature[50–57]. Table 2 summarizes the quantities, type of chemical and specification for solvents used in the dispersion of these LD materials into unit area of PSCs. Furthermore, the material and energy required for the synthesis of graphene-related materials and MoS_2 were directly taken from the previous studies [62,64,65,69] whereas for BP production, we prepared the inventories based on the previous experimental study[70]. All the inventories for the synthesis of unit mass of LD materials are shown in Table 3. All LCA models for all the PV technologies and LD materials were subsequently created using the GaBi software[46] and using the data from Ecoinvent V.3.8[71]database.

The lifetime and PCE of *ld*-PSC have varied in previous studies (see Table 1)[21,35,36]. These studies found that *ld*-PSCs retained more than 80% of their initial PCE after 30-45 days, whereas control PSCs retained only 50%. The lifespan of both PSCs and *ld*-PSC was unknown, ranging from 1 to 25 years in the literature[72]. Given these uncertainties, the study made the following assumptions: The initial PCE of both the PSC and *ld*-PSC was set at 25%. The average lifetime PCE of *ld*-PSC is ~22%, taking into account an 80% retention of initial PCE, while reference PSC maintains an average PCE of ~19% with only 50% of their initial PCE retained. The projected lifespan for PSCs is 25 years, whereas *ld*-PSCs were assumed to experience a 15% increase in lifetime, extending to 28.75 years. The lifespan and PCE of *ld*-PSC values were uncertain which impacts the robustness of LCA results. To enhance the robustness of impact results, we performed a sensitivity analysis for both the PCE and lifetime. Given that the average PCE of the reference PSC is 19%, we explored a range of PCE values for *ld*-PSC starting from 19% (assuming no PCE improvement) and extended up to 27.5%. Additionally, we also explored a broad range of lifetimes for *ld*-PSC in sensitivity analysis, spanning from 5 to 35 years.

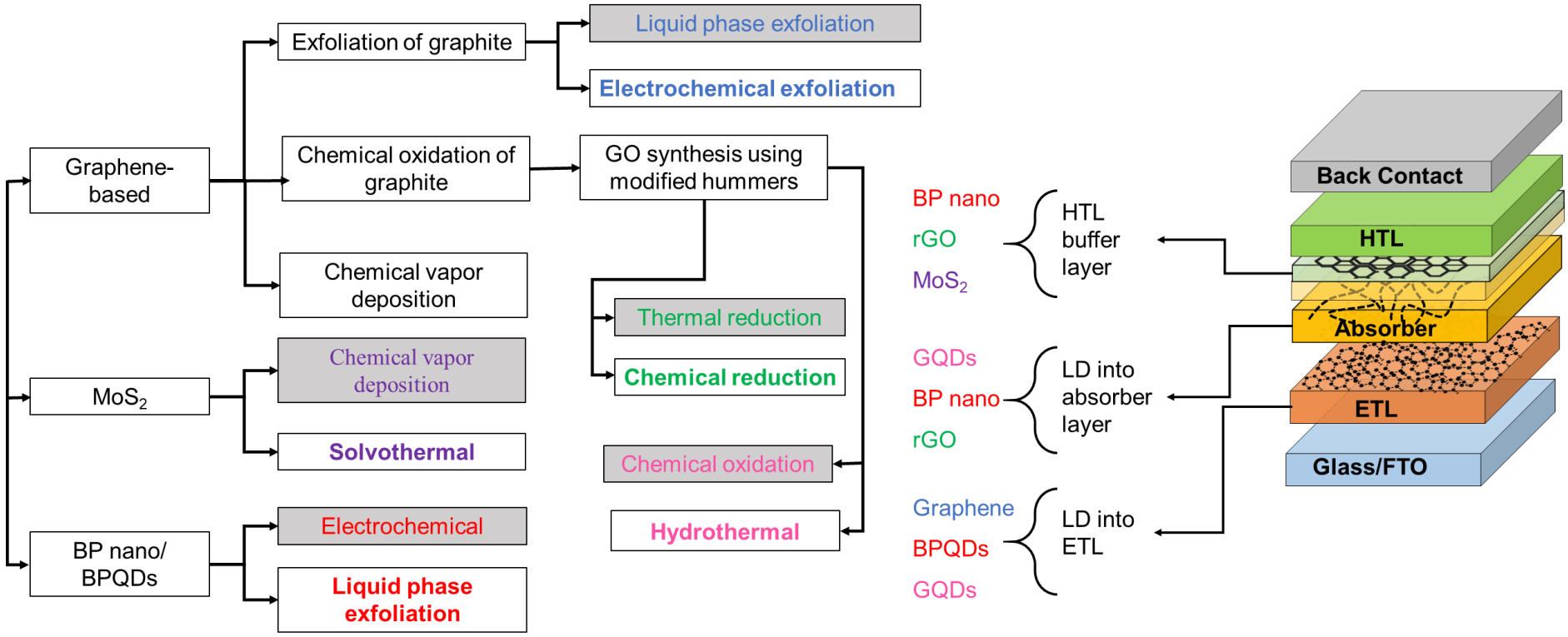

Figure 1. *Various LD material integration into PSC structure and possible synthesis routes. The color-coded processes represent possible synthesis routes, with bold colored ones indicating the selected routes for LD materials in this study. The processes highlighted in grey color have been excluded from consideration due to their impracticality for commercial-scale production, as they are both energy and time-intensive.*

Table 2 Inventory for various LD materials and chemicals used for the dispersion of these LD materials into ETL, HTL, and absorber layers of PSCs. The mass of all the materials was calculated for 1 m^2 of the PSC module. DMF-Dimethyl formamide, DMAc-Dimethylacetamide, IPA- Isopropyl alcohol.

Layer	LD	LD materials/ Chemicals	Mass	Units	Comments	Reference
ETL	Graphene	Graphene	22.7	mg	1 vol% of graphene in SnO_2 solution	48,73
		Ethanol	8.0	g	1 g of graphene in 354 g ethanol	
	GQDs	GQD	5.2	mg	1 wt % of GQDs in SnO_2 solution	74
		Water	5.3	g	1mg/ml of GQDs in water	
	BPQDs	BPQDs	3	mg	SnO_2 with 1.5 Mm BPQDs concentration	55
		Ethanol	4.8	g	0.5mg/ml of BPQDs in ethanol	
Absorber Layer	rGO	rGO	1.4	g	0.14 mg of rGO doped into 645 mg of perovskite	51
		DMF	6580	g	0.2 mg/ml of rGO in DMF	
	GQDs	GQDs	47	mg	GQDs concentration in perovskite solution is 7 vol%	52
		DMAc	29.3	g	0.93g/ml of GQDs in DMAc	
	BP-nano	BP-nano	2.6	mg	Assumed 1 wt% of BP in perovskite solution	56
		DMF	2.5	g	0.1mg/ml of BP-nano in DMF	
HTL	rGO	rGO	2.6	mg	Assumed 1 wt% of rGO in Spiro-OMeTAD solution	75
		Chlorobenzene	1.45	g	2mg/ml of rGO in chlorobenzene	
	BP-nano	BP-nano	60	mg	400 ml of BP solution with a concentration of 6 mg/ml	70
		IPA	8	g	0.78g/ml of BP-nano in IPA	
	MoS_2	MoS_2	0.25	g	MoS_2 layer thickness is 50nm	54,76,77
		IPA	981	g	0.2mg/ml of MoS_2 in IPA	

Table 3 Material and energy inventories required for the production of 1g of various LD materials.

LD materials		Materials/Energy	Value	Units	References
Graphene	Output	Graphene dispersion	1	g	[62]
	Inputs	Anode, graphite	3.91	g	
		Electricity, medium voltage	1.85	MJ	
		Potassium hydroxide	1.12	g	
		Water, deionized	670	g	
GO	Output	GO	1	g	[62]
	Inputs	Electricity, medium voltage	0.01	MJ	
		Graphite	0.71	g	
		Hydrogen peroxide (100%)	1.24	g	
		Potassium permanganate	2.14	g	
		Sodium nitrate	0.36	g	
		Sulfuric acid	30	g	
		Water, deionized	223	g	
rGO	Output	rGO	1	g	[62]
	Inputs	GO	1.25	g	
		Electricity, medium voltage	0.38	MJ	
		Ammonia	0.34	g	
		Methanol	10	g	
		Hydrazine	1.40	g	
		Water, deionized	163	g	
GQDs	Output	GQDs	1	mg	[64]
	Inputs	GO	20	mg	
		Potassium hydroxide	440	mg	
		Water, deionized	240	g	
		Electricity, medium voltage	0.20	kWh	
MoS_2	Output	MoS_2	1	g	[65]
	Inputs	Molybdenum	1.14	g	
		Hydrazine	20.23	g	
		Sodium hydroxide	11.52	g	
		elemental sulfur	0.52	g	
		ammonium carbonate	0.62	g	
		Ethylenediamine	199	g	
		Water, deionized	100	g	
		Acetone	150	g	
		Electricity, medium voltage	0.01	kWh	
BP-nano/ BPQDs	Output	BP-nano/BPQDs	1	g	[53]
	Inputs	Bulk BP crystal	2.85	g	
		N-Methyl Pyrrolidinone	1.42	kg	
		Isopropyl alcohol	157	g	
		Electricity, medium voltage	0.05	kWh	

3. Results

3.1. Environmental impacts comparison between LD materials

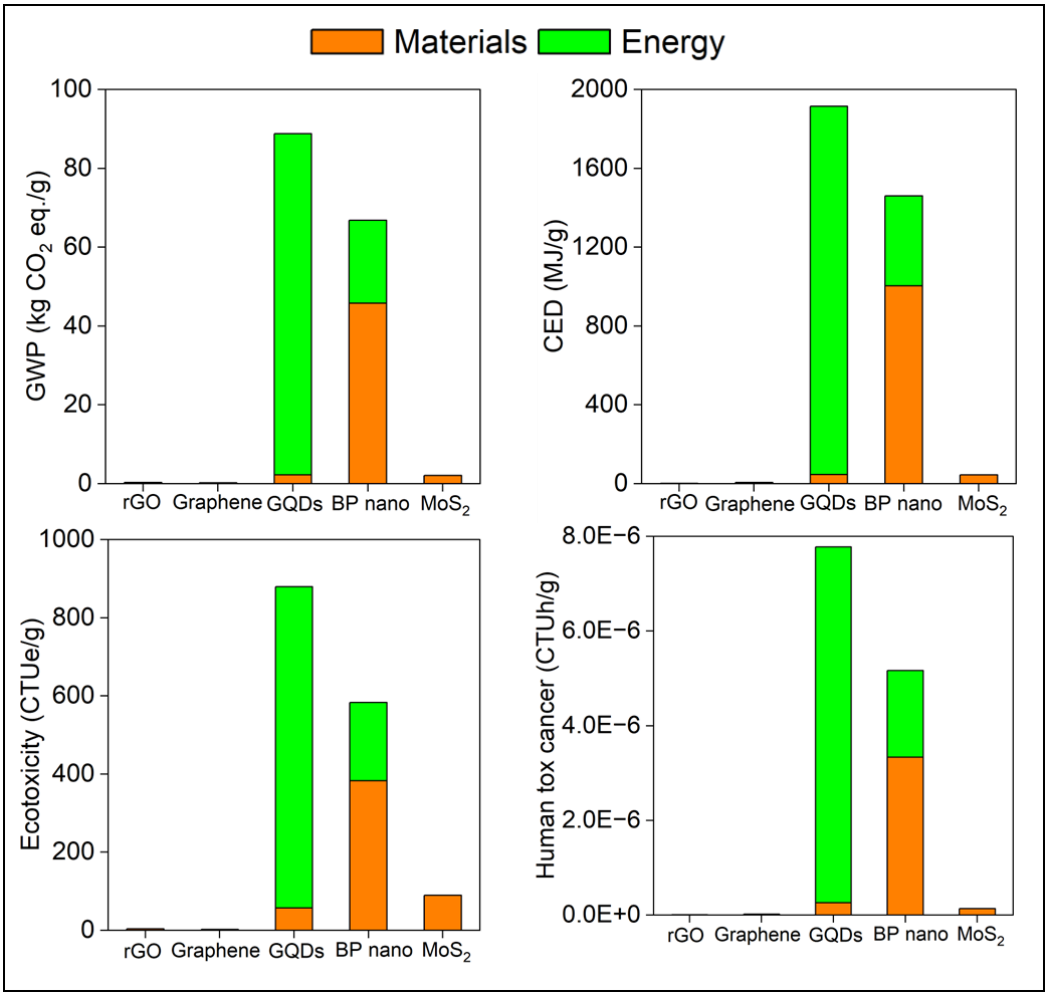

Figure 2. *Environmental impacts associated with materials and energy utilized in the synthesis of 1g of various LD materials across GWP, CED, ecotoxicity, and human toxicity (cancer) categories.*

Figure 2 shows the impacts of producing a unit mass of LD materials for four commonly reported environmental impact categories, namely GWP, CED, ecotoxicity, and human toxicity-cancer (see Table S.1 for all the remaining environmental impact categories). Across all four assessed categories, GQDs and BP-nano show a significantly higher environmental impact while rGO and graphene have negligible impacts. For GQDs, over 90% of environmental impacts across four categories can be attributed to energy used in synthesis. This is because the direct electricity consumed in the continuous hydrothermal process is sourced from a single batch and for a small quantity of GQDs [64]. For BP-nano's environmental impacts, the synthesis of bulk BP crystals relies on white phosphorus, which contributes around 50% in all four impact categories. The impacts associated with white phosphorous are due to the substantial consumption of phosphate rock and electricity during the synthesis process. Following closely, the second most significant factor contributing to the environmental impacts of BP-nano is the electricity consumption during the exfoliation and solvent exchange process of BP nanosheets, which varies between 30-35% across

the four impact categories. The remaining 10-20% of BP-nano impacts in four impact categories are associated with the N-methyl pyrrolidone solvent used for the exfoliation of bulk BP crystals. The production of a unit mass of MoS_2 shows significantly lower environmental impacts than GQDs and BP-nano across all four impact categories. In terms of MoS_2's GWP, CED, and human toxicity/cancer impacts, the primary contributor is the ethylenediamine solvent used in the autoclave during the synthesis process. On the other hand, the utilization of hydrazine in the synthesis of MoS_2 dominates the ecotoxicity impacts.

3.2. Environmental impacts comparison between LD materials incorporated into PSCs

Two alternative (Alt) configurations of *ld*-PSC have been analyzed to discuss the environmental impacts of the integration of LD materials into the PSC. Alt-1 contains graphene in the ETL, BP in the absorber layer, and rGO in the HTL, and Alt-2 incorporates GQDs in the ETL, rGO in the absorber layer, and BP in the HTL. Figure 3 shows the contributions of the average impacts resulting from the main components of *ld*-PSCs such as from PSC part and LD materials. We found that the impacts from LD materials incorporated into Alt-1 have a negligible contribution (<0.5%) to the overall impacts, whereas LD materials integrated into Alt-2 contributed to ~30% of the overall impacts. The substantial impact of LD materials in Alt-2 arises from both the considerable quantity of the LD materials integrated and chemicals used for the dispersion of these materials into Alt-2 configuration. For example, integration of rGO into the absorber layer of Alt-2 configuration requires a larger volume of DMF solvent during the dispersion process, accounting for 27% of the overall impacts of Alt-2 configuration. These impacts are predominantly linked to the organic compound dimethylamine, which is utilized in the synthesis of DMF. This finding emphasizes the critical importance of carefully choosing the dispersion chemical for *ld*-PSC. The BP-nano integrated into HTL has moderate impacts on the environmental performance of Alt-2; this is due to an upstream process such as the white phosphorous consumption in the synthesis of bulk BP crystals. The incorporation of GQDs in ETL has the least contribution to the overall impacts from Alt-2 and these minor impacts are primarily associated with electricity utilized in the synthesis of GQDs. To sum up, these results indicate that Alt-1 employing graphene in the ETL, BP in the absorber layer, and rGO in the HTL is the most promising configuration for sustainable PSC design in future energy generation.

In Table 4, we compared the environmental performance of unit electricity generated from Alt-1 and Alt-2 systems with other commercial PV technologies and PSC, as well as provided a detailed analysis regarding the impacts of them each environmental category, captured in the US EPA TRACI. PSC is used as a reference point for this analysis. Our results show that Alt-1 has the lowest, and c-Si has the highest impacts among almost all environmental categories which leads Alt-1 to be the most environmentally preferable PV structure, according to the average normalized environmental impacts. The environmental performance of Alt-1 is about ~25% and 40% better than PSC, and Alt-2, respectively. The improved environmental performance of Alt-1 compared to PSC is essentially a result of improvements in lifetime and PCE since the incorporation of LD materials into the PV structure has negligible impacts. The improved performance of Alt-1 compared to Alt-2 is a result of lower impacts, particularly in acidification, GWP, ozone depletion, eutrophication and resources, and fossil fuels categories. Alt-2 contains rGO in the absorber layer which contributes 30 to 50 % of each of these categories. In addition, the white phosphorus that is necessary for the synthesis of BP-nano, which is integrated into HTL, contributes to the impacts

of up to 7 % across ozone depletion, eutrophication, resources, and fossil fuels categories. Next, the mass of rGO in the absorber layer, and BP-nano in the HTL overlayer of Alt-2 is nearly 20 times and 500 times more than the mass of BP-nano in the absorber layer and rGO in HTL of Alt-1. Because of these significantly lower quantities of LD materials in HTL and absorber layers, Alt-1 has better environmental performance in all impact categories than Alt-2. Compared to commercial PV technologies, Alt-1 has significantly lower impacts in almost all impact categories except for ecotoxicity and human toxicity (non-cancer) categories, where CdTe and CIGS score better. The production of single-Si cells and aluminum alloy majorly contributed to significantly higher impacts of c-Si PV across all impact categories. In the context of CIGS, ozone depletion impacts are nearly four times higher compared to Alt-1. This notable increase in this impact category can be associated with polyethylene terephthalate used in the encapsulation of CIGS modules. The utilization of solar glass and aluminum alloy in CIGS is 1.5 to 2 times higher than the Alt-1 PSC configuration, which is responsible for higher impacts of CIGS compared to Alt-1 in the remaining impact categories. The adverse environmental performance of CdTe compared to Alt-1, is attributed to its higher impacts, especially in GWP, human health particularly air, ozone depletion and resources, and fossil fuel impact categories. The cause of these higher impacts in these categories is due to the higher electricity used in CdTe manufacturing (almost four times that of Alt-1). In addition, the improved environmental performance of Alt-1 compared to commercial PV technologies can also be attributed to enhanced PCE and extended lifetime resulting from the incorporation of LD materials.

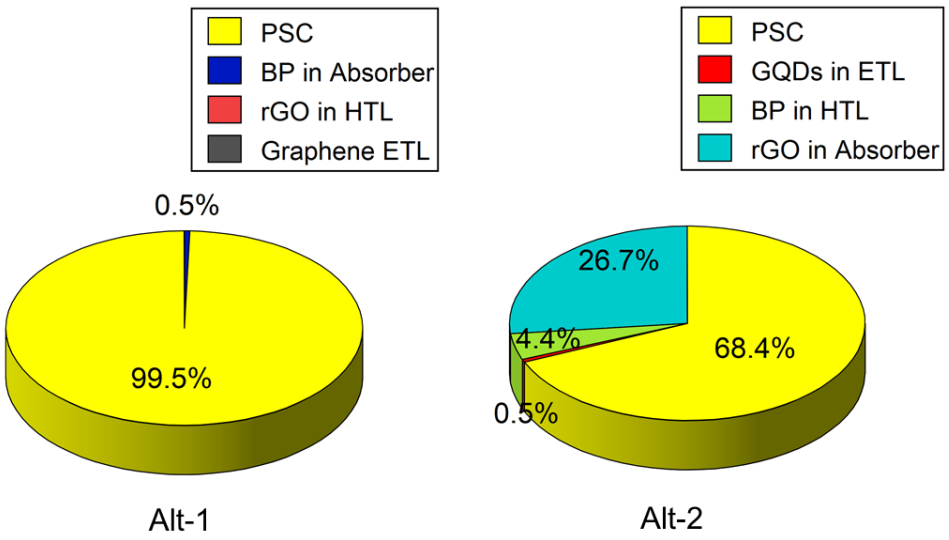

Figure 3. *The breakdown of environmental impacts by each component of Alt-1 and Alt-2 ld-*PSC *on overall average impacts. The environmental impacts of each component for 1m^2 of the ld-*PSC *module were calculated for all impact categories. The average contribution of each component is calculated according to Celik et al*[78] *. The raw data for each component for 1m^2 is also provided in Table S.2-S.5.*

Table 4 Comparison of the normalized environmental impacts of PSCs with commercial PV technologies. The results are normalized with the environmental impacts of reference PSC technology. The raw data for remaining PV technologies can be extracted using representative multipliers derived from baseline data of reference PSC, as provided in the last column. The equation for converting 1 m^2 of impacts to kWh impacts is provided in Eq S.1[15]. The average normalized impacts were determined by taking the mean of ten impact categories, following an approach similar to Celik et al [78]. In the Alt-1 *ld*-PSC configuration, the ETL incorporates graphene, the absorber layer integrates BP, and the HTL involves rGO. The Alt-2 *ld*-PSC comprises the inclusion of GQDs in ETL, rGO in the absorber layer, and BP in HTL. Alternative HTL material i.e., inorganic CuSCN-based *ld*-PSC configuration in comparison to Alt-1 configuration also assessed in Table S.8. PCE and lifetime values of CdTe, CIGS, c-Si, and PSC are directly taken from PVPS TASK 12 report[45]. An additional comparison between Alt-1 and inverted *ld*-PSC configuration, integrated with LD materials is also presented in Table S.9.

		Commercial PV			**Perovskite PV**			
	PV technology	**CdTe**	**CIGS**	**c-Si**	**Alt-1**	**Alt-2**	**PSC**	**PSC impacts/ kWh**
	PCE	18%	16%	20%	22%	22%	19%	
	Lifetime (years)	25	25	25	28.75	28.75	25	
Impact Category	Acidification	0.75	1.27	1.77	0.75	1.32	1.00	5.70E-05 (kg SO_2-eq)
	Ecotoxicity	0.39	0.63	1.08	0.75	0.79	1.00	9.62E-01 (CTUe)
	Eutrophication	0.79	0.72	2.77	0.76	1.20	1.00	4.06E-05 (kg N-eq)
	GWP	1.28	1.99	2.78	0.76	1.25	1.00	6.01E-03 (kg CO_2-eq)
	Human health particulate air	1.21	1.34	2.74	0.76	1.04	1.00	1.34E-05 (kg $PM_{2.5}$-eq)
	Human toxicity, cancer	0.95	1.43	1.40	0.75	0.91	1.00	1.26E-09 (CTUh)
	Human toxicity, non-canc.	0.24	0.45	1.04	0.75	0.82	1.00	1.02E-08 (CTUh)
	Ozone depletion air	1.07	3.52	2.66	0.76	1.56	1.00	6.16E-10(kg CFC 11-eq)
	Resources, fossil fuels	1.12	1.91	2.13	0.76	1.70	1.00	8.15E-03 (MJ surplus energy)
	Smog air	0.82	1.62	1.68	0.75	0.98	1.00	6.56E-04 (kg O_3-eq)
	Average Normalized Impact	**0.86**	**1.50**	**2.00**	**0.75**	**1.15**	**1.00**	
	CED	1.22	1.68	2.72	0.76	1.50	1	1.10E-01 (MJ)

most environmentally preferable	<0.70
more environmentally preferable	0.71-0.85
Neutral	0.86-1.14
less environmentally preferable	1.15-1.29

least environmentally preferable	>1.30

1

3.3 Sensitivity analysis

To further explore the impacts of lifetime and PCE on the average normalized environmental impacts of Alt-1 and Alt-2 *ld*-PSC, we independently varied these parameters and pointed out the technological development in terms of PCE and lifetime that these PVs outperform conventional PVs and PSCs (Figure 4). The findings from this analysis reveal that Alt-1 does not require any enhancement in terms of lifetime and PCE, whereas Alt-2 requires significant improvements in both lifetime and PCE to outperform the environmental performance of reference PSC and certain commercial PV technologies. For Alt-2 *ld*-PSC to achieve an environmental impact equivalent to PSC, it would require a minimum of a 27-year lifetime and PCE of at least 27.5%. Similarly, to outperform the environmental performance of CdTe, Alt-2 *ld*-PSC would need a minimum lifetime of 31 years and a PCE of 27.5%.

Furthermore, it's worth noticing that Alt-1 *ld*-PSC can surpass the environmental performance of commercial PV technologies, even when functioning with reduced lifetimes (Figure 4. A). To determine the break-even lifetime of Alt-1 *ld*-PSC, the following equation is used:

$$Impact_{Alt-1} \times \frac{25}{Lifetime_{Alt-1}} = Impact_{comm} \qquad Eq.1$$

where $Impact_{Alt\text{-}1}$ and $Impact_{comm}$ are the average normalized impact of the Alt-1 *ld*-PSC and commercial PV technologies, and $Lifetime_{Alt\text{-}1}$ is the lifetime of Alt-1 *ld*-PSC. The commercial PV technology's lifetime is assumed to be 25 years. For example, Alt-1 *ld*-PSC with 20% PCE would need a lifetime of only 10.3, 13.8, and 24 years to outperform the environmental performance of c-Si, CIGS, and CdTe technologies respectively, which is currently shorter than the PSC lifetime (25 years). Therefore, the incorporation of LD materials like graphene in the ETL, BP in the perovskite layer, and rGO in HTL of Alt-1 demonstrates significant potential for the commercial applications of PSC. This is due to their ability to align with the environmental performance of PSC and commercial PV technologies, even within a shorter lifetime.

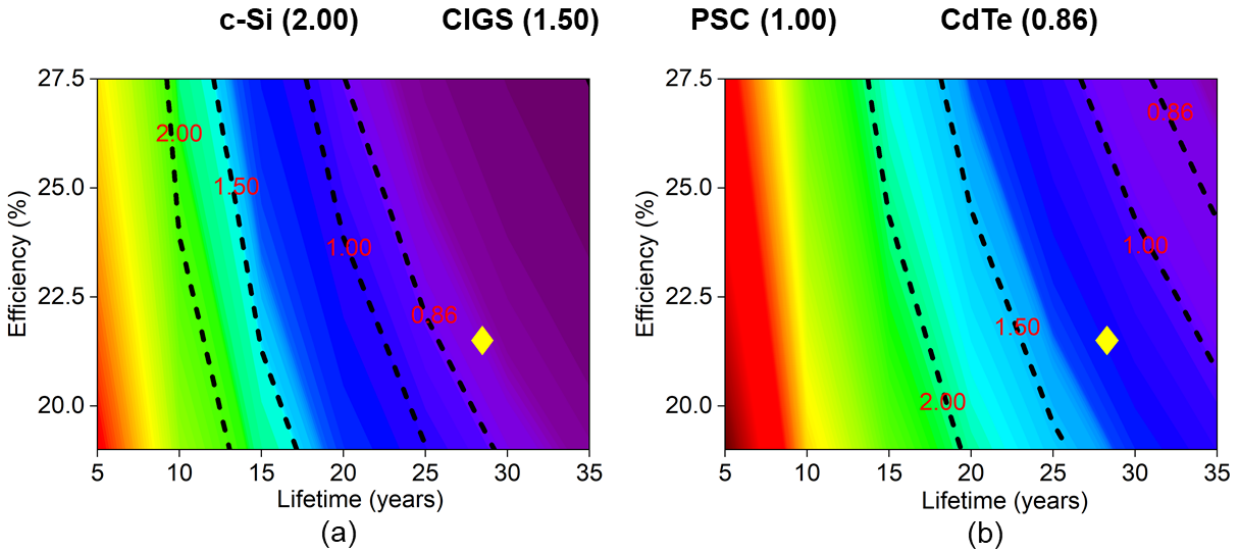

Figure 4. *The influence of PCE and lifetime on the average normalized environmental impacts of Alt-1(a) and Alt-2(b) ld-PSC. The diamond icon (yellow) represents the average normalized environmental impact of Alt-1 ld-PSC*

(i.e., 0.76) and Alt-2 ld-PSC (1.16), corresponding to the current lifetime and PCE. The average normalized environmental impact of c-Si, CdTe, and CIGS is 2.00, 0.86, and 1.50 respectively (as outlined in Table 4). Additionally, Figure 4.a and 4. b also show the environmental impact of ld-PSC equivalent to PSC and commercial technologies in black dashed lines.

3.4 GWP impacts and EPBT: comparison with commercial PV technologies.

The GWP impacts, also known as carbon footprint, and EPBT (see Eq. S2) values of electricity generated from *ld*-PSC, along with a comparative analysis against PSC and commercial PV technologies are shown in Figure 5. Overall, Alt-1 *ld*-PSC has lower GWP and EPBT values than PSC and commercial PV technologies. The GWP impacts of various PV technologies range from ~ 4.5 to 17 g $CO_{2\ eq}$/kWh. Among the various PV technologies analyzed, Alt-1 *ld*-PSC exhibits lower GWP impacts, while c-Si PV shows comparatively higher GWP impacts. The GWP impact of Alt-1 *ld*-PSC is 4.5 g CO_2 eq/kWh, which is ~20- 40% lower than PSC and Alt-2 *ld*-PSC technologies, and ~40-75% lower than commercial PV technologies. We further compared the GWP impacts of PSC and commercial PV technologies with recent literature findings. Leccisi et al. reported GWP impacts of PSC, CdTe, and CIGS PV technologies in terms of m^2 of PV panels [9]. To facilitate a meaningful comparison with our study, we converted these GWP impacts from m^2 to kWh impacts, assuming comparable irradiation levels, PCE, performance ratio, and lifetime parameters as used in our study. The GWP impacts of PSC, CdTe, and CIGS technologies as calculated according to Leccisi et al were 5.3, 9.0, and 18.5 g $CO_{2\ eq}$/kWh, respectively. The GWP values obtained for PSC and commercial PV technologies in our study show slight variations when compared to the findings reported by Leccisi et al. Specifically, our study reveals that the GWP impacts of PSC technology are approximately 15% higher than the values documented by Leccisi et al. This disparity can be attributed to the utilization of different materials and deposition methods during the synthesis of PSC. For instance, in the study conducted by Leccisi et al., they examined PSC structure utilizing CuSCN as HTL and molybdenum coupled with aluminum as BC. They employed a spray coating deposition method for PSC fabrication. In contrast, our study involves spiro-OMeTAD as HTL and silver as BC, with a slot die coating method used as a deposition method. For c-Si impacts, we compared our study results with the most recent LCA study conducted by Fthenakis et al, which employed updated c-Si PV data[8]. Fthenakis reported a GWP of 22 g $CO_{2\ eq}$/kWh for c-Si, which is ~35% higher than the GWP impacts found in our study (17 g $CO_{2\ eq}$/kWh)[8]. This is because we used a United States electricity mix source compared to the Chinese electricity mixture used in Fthenakis et al. Note that according to TRACI method, the GWP impacts of 1 kWh of electricity production in the US and China are calculated to be 0.4 and 0.9 kg $CO_{2\ eq}$/kWh, respectively, this difference could be responsible for disparities between our study findings and theirs.

The EPBT value of *ld*-PSC varies from approximately three to six months, whereas commercial technologies range from four to nine months (Figure 5). The Alt-1 *ld*-PSC has the lowest EPBT (2.8 months) among the analyzed PV technologies, while c-Si PV requires around nine months. The EPBT values of commercial PV technologies determined in this study are slightly lower compared to the findings from Leccisi et al and Fthenakis et al [8,9]. This variation can be attributed to the embedded energy used in the EPBT calculations, which varies based on factors such as the materials and deposition methods used in synthesis, the country specific electricity mixes and associated characterization factors.

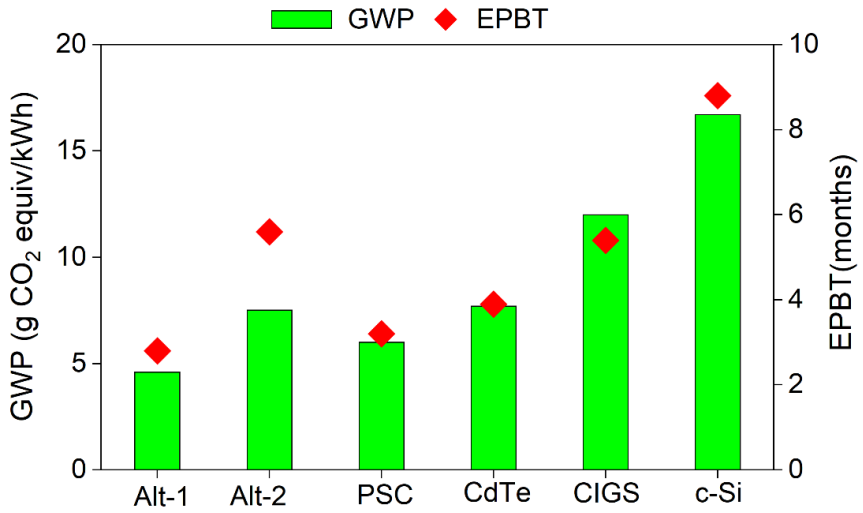

Figure 5. *Comparison of GWP and EPBT of Alt-1 and Alt-2 ld-*PSC *with reference PSC and other commercial PV technologies. These comparisons are made under the assumption of an average global solar irradiation of 1700 kWh/m^2/yr. and a performance ratio of 0.75.*

4. Conclusions

In this study, we considered five LD materials that are frequently investigated for the integration of PSC: graphene, rGO, GQDs, MoS_2, and BP. A unit mass-based LD materials comparison reveals that rGO, graphene, and MoS_2 are the most environmentally friendly options. However, the environmental impact of these materials undergoes significant when integrated into *ld*-PSC configurations, depending on the type and quantity of chemicals used for the dispersion. This emphasizes the critical importance of carefully choosing the chemicals used for dispersion. For the assessment of the environmental performance of *ld*-PSC following the incorporation of various LD materials, we selected two distinct *ld*-PSC configurations and conducted a comparative analysis with reference PSC and commercial PV technologies. Our results show that Alt-1 *ld*-PSC configuration which incorporates graphene in the ETL, BP in perovskite, and rGO in HTL layers has ~20% lower average environmental impacts compared to PSC. Conversely, the Alt-2 *ld*-PSC configuration that employs GQDs in ETL, rGO in the absorber layer, and BP in the HTL layer showed ~15% more average impacts than PSC. Furthermore, this study also highlighted that Alt-1 *ld*-PSC configuration operating at a benchmark PCE of 20%, demonstrated the potential to outperform c-Si, CIGS, and CdTe technologies at a lower lifetime of only 10.3, 13.8, and 24 years, respectively. Moreover, the investigation of significant sustainability metrics, such as energy payback time, demonstrated that with *ld*-PSC, the energy can be paid back in a time period up to three times shorter than commercial PV technologies. The findings of the study emphasize the significance of Alt-1 *ld*-PSC as a sustainable PSC configuration that can outperform established commercial PV technologies.

Acknowledgments

This work is partially funded by the US National Science Foundation's Grants # 2138293 and 2239755. We thank Dr. Venkata Ramana Gadhamshetty for his valuable comments in the initial phase of the development of this work.

References:

1 International Energy Agency, *Snapshot of Global PV Markets 2023. Task 1 Strategic PV Analysis and Outreach. IEA PVPS*, Paris, France, 2023, vol. I.

2 International Energy Agency, *Tracking SDG7: The Energy Progress Report 2023*, Paris, France, 2023.

3 Statista, Global solar energy share in electricity mix 2022, https://www.statista.com/statistics/1302055/global-solar-energy-share-electricity-mix/, (accessed 30 October 2023).

4 DNV, Energy Transition Outlook - 2023, https://www.dnv.com/energy-transition-outlook/index.html, (accessed 1 November 2023).

5 J. Pastuszak and P. Węgierek, Photovoltaic Cell Generations and Current Research Directions for Their Development, *Materials (Basel).*, , DOI:10.3390/ma15165542.

6 S. Suragtkhuu, S. Sunderiya, P. Myagmarsereejid, S. Purevdorj, A. S. R. Bati, B. Bold, Y. L. Zhong, S. Davaasambuu and M. Batmunkh, Graphene-Like Monoelemental 2D Materials for Perovskite Solar Cells, *Adv. Energy Mater.*, , DOI:10.1002/aenm.202204074.

7 National Renewable Energy Laboratory (NREL), Best Research-Cell Efficiency Chart | Photovoltaic Research | NREL, https://www.nrel.gov/pv/cell-efficiency.html, (accessed 17 October 2023).

8 V. Fthenakis and E. Leccisi, Updated sustainability status of crystalline silicon-based photovoltaic systems: Life-cycle energy and environmental impact reduction trends, *Prog. Photovoltaics Res. Appl.*, 2021, **29**, 1068–1077.

9 E. Leccisi and V. Fthenakis, Life cycle energy demand and carbon emissions of scalable single-junction and tandem perovskite PV, *Prog. Photovoltaics Res. Appl.*, 2021, **29**, 1078–1092.

10 A. Maalouf, T. Okoroafor, Z. Jehl, V. Babu and S. Resalati, A comprehensive review on life cycle assessment of commercial and emerging thin-film solar cell systems, *Renew. Sustain. Energy Rev.*, 2023, **186**, 113652.

11 I. Celik, Z. Song, A. J. Cimaroli, Y. Yan, M. J. Heben and D. Apul, Life Cycle Assessment (LCA) of perovskite PV cells projected from lab to fab, *Sol. Energy Mater. Sol. Cells*, 2016, **156**, 157–169.

12 J. Y. Kim, J.-W. Lee, H. S. Jung, H. Shin and N.-G. Park, High-Efficiency Perovskite Solar Cells, *Chem. Rev.*, 2020, **120**, 7867–7918.

13 J. Zhang, N. Chang, C. Fagerholm, M. Qiu, L. Shuai, R. Egan and C. Yuan, Techno-economic and environmental sustainability of industrial-scale productions of perovskite solar cells, *Renew. Sustain. Energy Rev.*, , DOI:10.1016/j.rser.2022.112146.

14 N. Kwon, J. Lee, M. J. Ko, Y. Y. Kim and J. Seo, Recent progress of eco-friendly manufacturing process of efficient perovskite solar cells, *Nano Converg.*, , DOI:10.1186/s40580-023-00375-5.

15 I. Celik, A. B. Phillips, Z. Song, Y. Yan, R. J. Ellingson, M. J. Heben and D. Apul, Environmental analysis of perovskites and other relevant solar cell technologies in a tandem configuration, *Energy Environ. Sci.*, 2017, **10**, 1874–1884.

16 P. Čulík, K. Brooks, C. Momblona, M. Adams, S. Kinge, F. Maréchal, P. J. Dyson and M. K. Nazeeruddin, Design and Cost Analysis of 100 MW Perovskite Solar Panel Manufacturing Process in Different Locations, *ACS Energy Lett.*, 2022, 3039–3044.

17 I. Celik, R. Hosseinian Ahangharnejhad, Z. Song, M. Heben and D. Apul, Emerging Photovoltaic (PV) Materials for a Low Carbon Economy, *Energies*, 2020, **13**, 4131.

18 J. Zheng, W. Duan, Y. Guo, Z. C. Zhao, H. Yi, F. J. Ma, L. Granados Caro, C. Yi, J. Bing, S. Tang, J. Qu, K. C. Fong, X. Cui, Y. Zhu, L. Yang, A. Lambertz, M. Arafat Mahmud, H. Chen, C. Liao, G. Wang, M. Jankovec, C. Xu, A. Uddin, J. M. Cairney, S. Bremner, S. Huang, K. Ding, D. R. McKenzie and A. W. Y. Ho-Baillie, Efficient monolithic perovskite-Si tandem solar cells enabled by an ultra-thin indium tin oxide interlayer, *Energy Environ. Sci.*, 2023, **16**, 1223–1233.

19 A. W. Y. Ho-Baillie, J. Zheng, M. A. Mahmud, F. J. Ma, D. R. McKenzie and M. A. Green, Recent progress and future prospects of perovskite tandem solar cells, *Appl. Phys. Rev.*, ,

DOI:10.1063/5.0061483.
20 A. S. R. Bati, M. Batmunkh and J. G. Shapter, Emerging 2D Layered Materials for Perovskite Solar Cells, *Adv. Energy Mater.*, , DOI:10.1002/aenm.201902253.
21 M. Alzaid, Recent progress in the role of two-dimensional materials as an efficient charge transport layer in perovskite solar cells, *Int. J. Energy Res.*, 2021, **45**, 12598–12613.
22 S. O. Ali Ahmad, A. Ashfaq, M. U. Akbar, M. Ikram, K. Khan, F. Wang, M. Ikram and A. Mahmood, Application of two-dimensional materials in perovskite solar cells: recent progress, challenges, and prospective solutions, *J. Mater. Chem. C*, 2021, **9**, 14065–14092.
23 C. C. Boyd, R. Cheacharoen, T. Leijtens and M. D. McGehee, Understanding Degradation Mechanisms and Improving Stability of Perovskite Photovoltaics, *Chem. Rev.*, 2019, **119**, 3418–3451.
24 D. Zhang, D. Li, Y. Hu, A. Mei and H. Han, Degradation pathways in perovskite solar cells and how to meet international standards, *Commun. Mater.*, , DOI:10.1038/s43246-022-00281-z.
25 G. Jeong, D. Koo, J. Seo, S. Jung, Y. Choi, J. Lee and H. Park, Suppressed interdiffusion and degradation in flexible and transparent metal electrode-based perovskite solar cells with a graphene interlayer, *Nano Lett.*, 2020, **20**, 3718–3727.
26 S. Wu, R. Chen, S. Zhang, B. H. Babu, Y. Yue, H. Zhu, Z. Yang, C. Chen, W. Chen, Y. Huang, S. Fang, T. Liu, L. Han and W. Chen, A chemically inert bismuth interlayer enhances long-term stability of inverted perovskite solar cells, *Nat. Commun.*, 2019, **10**, 1–11.
27 M. Dehghanipour, A. Behjat and H. Amrollahi Bioki, Fabrication of stable and efficient 2D/3D perovskite solar cells through post-treatment with TBABF4, *J. Mater. Chem. C*, 2021, **9**, 957–966.
28 A. R. Bin Mohd Yusoff, M. Vasilopoulou, D. G. Georgiadou, L. C. Palilis, A. Abate and M. K. Nazeeruddin, Passivation and process engineering approaches of halide perovskite films for high efficiency and stability perovskite solar cells, *Energy Environ. Sci.*, 2021, **14**, 2906–2953.
29 S. Tang, S. Peracchi, Z. Pastuovic, C. Liao, A. Xu, J. Bing, J. Zheng, M. A. Mahmud, G. Wang, E. D. Townsend-Medlock, G. J. Wilson, G. Lakhwani, C. Brenner, D. R. McKenzie and A. W. Y. Ho-Baillie, Effect of Hole Transport Materials and Their Dopants on the Stability and Recoverability of Perovskite Solar Cells on Very Thin Substrates after 7 MeV Proton Irradiation, *Adv. Energy Mater.*, 2023, **13**, 1–9.
30 C. A. R. Perini, E. Rojas-Gatjens, M. Ravello, A. F. Castro-Mendez, J. Hidalgo, Y. An, S. Kim, B. Lai, R. Li, C. Silva-Acuña and J. P. Correa-Baena, Interface Reconstruction from Ruddlesden–Popper Structures Impacts Stability in Lead Halide Perovskite Solar Cells, *Adv. Mater.*, , DOI:10.1002/adma.202204726.
31 C. A. R. Perini, A. F. Castro-Mendez, T. Kodalle, M. Ravello, J. Hidalgo, M. Gomez-Dominguez, R. Li, M. Taddei, R. Giridharagopal, J. Pothoof, C. M. Sutter-Fella, D. S. Ginger and J. P. Correa-Baena, Vapor-Deposited n = 2 Ruddlesden-Popper Interface Layers Aid Charge Carrier Extraction in Perovskite Solar Cells, *ACS Energy Lett.*, , DOI:10.1021/acsenergylett.2c02419.
32 T. Dai, Q. Cao, L. Yang, M. H. Aldamasy, M. Li, Q. Liang, H. Lu, Y. Dong and Y. Yang, Strategies for high-performance large-area perovskite solar cells toward commercialization, *Crystals*, , DOI:10.3390/cryst11030295.
33 U. K. Aryal, M. Ahmadpour, V. Turkovic, H. G. Rubahn, A. Di Carlo and M. Madsen, 2D materials for organic and perovskite photovoltaics, *Nano Energy*, , DOI:10.1016/j.nanoen.2021.106833.
34 M. Hadadian, J. H. Smått and J. P. Correa-Baena, The role of carbon-based materials in enhancing the stability of perovskite solar cells, *Energy Environ. Sci.*, 2020, **13**, 1377–1407.
35 P. You, G. Tang and F. Yan, Two-dimensional materials in perovskite solar cells, *Mater. Today Energy*, 2019, **11**, 128–158.
36 N. E. Safie, M. A. Azam, M. F. A. Aziz and M. Ismail, Recent progress of graphene-based materials for efficient charge transfer and device performance stability in perovskite solar cells, *Int. J. Energy Res.*, 2021, **45**, 1347–1374.
37 Z. Niazi, A. Hagfeldt and E. K. Goharshadi, Recent progress on the use of graphene-based

nanomaterials in perovskite solar cells, *J. Mater. Chem. A*, 2023, **11**, 6659–6687.
38 J. H. Heo, D. S. Lee, F. Zhang, C. Xiao, S. J. Heo, H. J. Lee, K. Zhu and S. H. Im, Super Flexible Transparent Conducting Oxide-Free Organic–Inorganic Hybrid Perovskite Solar Cells with 19.01% Efficiency (Active Area = 1 cm 2), *Sol. RRL*, , DOI:10.1002/solr.202100733.
39 Y. Wang, W. Li, Y. Yin, M. Wang, W. Cai, Y. Shi, J. Guo, W. Shang, C. Zhang, Q. Dong, H. Ma, J. Liu, W. Tian, S. Jin, J. Bian and Y. Shi, Defective MWCNT Enabled Dual Interface Coupling for Carbon-Based Perovskite Solar Cells with Efficiency Exceeding 22%, *Adv. Funct. Mater.*, , DOI:10.1002/adfm.202204831.
40 J. Yoon, H. Sung, G. Lee, W. Cho, N. Ahn, H. S. Jung and M. Choi, Superflexible, high-efficiency perovskite solar cells utilizing graphene electrodes: Towards future foldable power sources, *Energy Environ. Sci.*, 2017, **10**, 337–345.
41 A. S. R. Bati, Y. L. Zhong, P. L. Burn, M. K. Nazeeruddin, P. E. Shaw and M. Batmunkh, Next-generation applications for integrated perovskite solar cells, *Commun. Mater.*, 2023, **4**, 1–24.
42 J. Bing, L. G. Caro, H. P. Talathi, N. L. Chang, D. R. Mckenzie and A. W. Y. Ho-Baillie, Perovskite solar cells for building integrated photovoltaics—glazing applications, *Joule*, 2022, **6**, 1446–1474.
43 ISO 14040:2006, Environmental management: Life cycle assessment; Principles and framework, https://www.iso.org/standard/37456.html, (accessed 7 September 2023).
44 ISO 14044:2006, Environmental management: Life cycle assessment; Requirements and guidelines, https://www.iso.org/standard/38498.html, (accessed 6 September 2023).
45 R. Frischknecht, P. Stolz, L. Krebs, M. de Wild-Scholten, P. Sinha, V. Fthenakis, C. Kim, M. Raugei and M. Stucki, *Life Cycle Inventories and Life Cycle Assessments of Photovoltaic Systems. International Energy Agency (IEA) PVPS Task12, Report T12-19*, 2020.
46 Sphera, Life Cycle Assessment Software. LCA for Experts (GaBi)., https://sphera.com/life-cycle-assessment-lca-software/, (accessed 7 September 2023).
47 J. Bare, *Tool for the Reduction and Assessment of Chemical and O ther Environmental Impacts (TRACI). User's Guide Tool for the Reduction and Assessment of Chemical and Other Environmental Impacts (TRACI)*, Washington, DC, USA, 2012, vol. 600/R–12/5.
48 M. Zhu, W. Liu, W. Ke, L. Xie, P. Dong and F. Hao, Graphene-Modified Tin Dioxide for Efficient Planar Perovskite Solar Cells with Enhanced Electron Extraction and Reduced Hysteresis, *ACS Appl. Mater. Interfaces*, 2019, **11**, 666–673.
49 N. A. A. Malek, N. Alias, A. A. Umar, X. Zhang, X. Li, S. K. M. Saad, N. A. Abdullah, H. Zhang, Z. Weng, Z. Shi, C. Li, M. M. Rosli and Y. Zhan, Enhanced Charge Transfer in Atom-Thick 2H–WS2 Nanosheets' Electron Transport Layers of Perovskite Solar Cells, *Sol. RRL*, , DOI:10.1002/solr.202000260.
50 R. Gui, H. Jin, Z. Wang and J. Li, Black phosphorus quantum dots: Synthesis, properties, functionalized modification and applications, *Chem. Soc. Rev.*, 2018, **47**, 6795–6823.
51 A. K. Kadhim, M. R. Mohammad and A. I. Abd Ali, Enhancing the efficiency of perovskite solar cells by modifying perovskite layer with rGO additive, *Chem. Phys. Lett.*, 2022, **786**, 2–6.
52 X. Fang, J. Ding, N. Yuan, P. Sun, M. Lv, G. Ding and C. Zhu, Graphene quantum dot incorporated perovskite films: Passivating grain boundaries and facilitating electron extraction, *Phys. Chem. Chem. Phys.*, 2017, **19**, 6057–6063.
53 S. K. Muduli, E. Varrla, S. A. Kulkarni, G. Han, K. Thirumal, O. Lev, S. Mhaisalkar and N. Mathews, 2D black phosphorous nanosheets as a hole transporting material in perovskite solar cells, *J. Power Sources*, 2017, **371**, 156–161.
54 A. Agresti, S. Pescetelli, A. L. Palma, B. Martín-García, L. Najafi, S. Bellani, I. Moreels, M. Prato, F. Bonaccorso and A. Di Carlo, Two-Dimensional Material Interface Engineering for Efficient Perovskite Large-Area Modules, *ACS Energy Lett.*, 2019, **4**, 1862–1871.
55 B. Gu, Y. Du, B. Chen, R. Zhao, H. Lu, Q. Xu and C. Guo, Black Phosphorus Quantum Dot-Engineered Tin Oxide Electron Transport Layer for Highly Stable Perovskite Solar Cells with Negligible Hysteresis, *ACS Appl. Mater. Interfaces*, 2022, **14**, 11264–11272.

56 Y. Wang, H. Zhang, T. Zhang, W. Shi, M. Kan, J. Chen and Y. Zhao, Photostability of MAPbI 3 Perovskite Solar Cells by Incorporating Black Phosphorus, *Sol. RRL*, , DOI:10.1002/solr.201900197.
57 S. Suragtkhuu, O. Tserendavag, U. Vandandoo, A. S. R. Bati, M. Bat-Erdene, J. G. Shapter, M. Batmunkh and S. Davaasambuu, Efficiency and stability enhancement of perovskite solar cells using reduced graphene oxide derived from earth-abundant natural graphite, *RSC Adv.*, 2020, **10**, 9133–9139.
58 W. Chen, K. Li, Y. Wang, X. Feng, Z. Liao, Q. Su, X. Lin and Z. He, Black Phosphorus Quantum Dots for Hole Extraction of Typical Planar Hybrid Perovskite Solar Cells, *J. Phys. Chem. Lett.*, 2017, **8**, 591–598.
59 P. You, G. Tang and F. Yan, Two-dimensional materials in perovskite solar cells Two-dimensional materials in perovskite solar cells, *Mater. Today Energy*, 2018, **11**, 128–158.
60 A. A. MOOSA and M. S. ABED, Graphene preparation and graphite exfoliation, *Turkish J. Chem.*, 2021, **45**, 493–519.
61 N. Kumar, R. Salehiyan, V. Chauke, O. Joseph Botlhoko, K. Setshedi, M. Scriba, M. Masukume and S. Sinha Ray, Top-down synthesis of graphene: A comprehensive review, *FlatChem*, 2021, **27**, 100224.
62 M. Cossutta, J. McKechnie and S. J. Pickering, A comparative LCA of different graphene production routes, *Green Chem.*, 2017, **19**, 5874–5884.
63 C. Zhao, X. Song, Y. Liu, Y. Fu, L. Ye, N. Wang, F. Wang and L. Li, *Synthesis of graphene quantum dots and their applications in drug delivery*, 2020.
64 S. Kellici, J. Acord, K. E. Moore, N. P. Power, V. Middelkoop, D. J. Morgan, T. Heil, P. Coppo, I. A. Baragau and C. L. Raston, Continuous hydrothermal flow synthesis of graphene quantum dots, *React. Chem. Eng.*, 2018, **3**, 949–958.
65 M. Hachhach, H. Akram, A. El Kasmi, M. Hanafi, O. Achak and T. Chafik, Life cycle assessment of large-scale production of MoS2 nanomaterials through the solvothermal method, *J. Nanoparticle Res.*, 2022, **24**, 1–14.
66 Y. Zeng and Z. Guo, Synthesis and stabilization of black phosphorus and phosphorene: Recent progress and perspectives, *iScience*, , DOI:10.1016/j.isci.2021.103116.
67 de Wild-Scholten, *Life Cycle Analysis of CHEOPS technologies and benchmarking: Screening*, SmartGreenScans, Groet, NL, 2017.
68 L. Ramseier, P. Stolz and R. Frischknecht, *Life Cycle Assessment of a Perovskite Silicon Tandem Photo-voltaic Panel. Swiss Federal Office of Energy SFOE*, Uster, Switzerland, 2019.
69 M. Cossutta, V. Vretenar, T. A. Centeno, P. Kotrusz, J. McKechnie and S. J. Pickering, A comparative life cycle assessment of graphene and activated carbon in a supercapacitor application, *J. Clean. Prod.*, , DOI:10.1016/j.jclepro.2019.118468.
70 S. K. Muduli, E. Varrla, S. A. Kulkarni, G. Han, K. Thirumal, O. Lev, S. Mhaisalkar, N. Mathews, K. Mahmood, A. Khalid, S. W. Ahmad, H. G. Qutab, M. Hameed, R. Sharif, F. A. Deorsola, N. Russo, G. A. Blengini, D. Fino, B. Gu, Y. Du, B. Chen, R. Zhao, H. Lu, Q. Xu and C. Guo, Black Phosphorus Quantum Dot-Engineered Tin Oxide Electron Transport Layer for Highly Stable Perovskite Solar Cells with Negligible Hysteresis, *J. Power Sources*, 2017, **203**, 1–6.
71 Ecoinvent, Ecoinvent v3.8, https://ecoinvent.org/the-ecoinvent-database/data-releases/ecoinvent-3-8/, (accessed 10 September 2023).
72 Z. Song, C. L. McElvany, A. B. Phillips, I. Celik, P. W. Krantz, S. C. Watthage, G. K. Liyanage, D. Apul and M. J. Heben, A technoeconomic analysis of perovskite solar module manufacturing with low-cost materials and techniques, *Energy Environ. Sci.*, 2017, **10**, 1297–1305.
73 S. Pescetelli, A. Agresti, G. Viskadouros, S. Razza, K. Rogdakis, I. Kalogerakis, E. Spiliarotis, E. Leonardi, P. Mariani, L. Sorbello, M. Pierro, C. Cornaro, S. Bellani, L. Najafi, B. Martín-García, A. E. Del Rio Castillo, R. Oropesa-Nuñez, M. Prato, S. Maranghi, M. L. Parisi, A. Sinicropi, R. Basosi, F. Bonaccorso, E. Kymakis and A. Di Carlo, Integration of two-dimensional materials-based perovskite solar panels into a stand-alone solar farm, *Nat. Energy*, 2022, **7**, 597–607.

74 J. Xie, K. Huang, X. Yu, Z. Yang, K. Xiao, Y. Qiang, X. Zhu, L. Xu, P. Wang, C. Cui and D. Yang, Enhanced Electronic Properties of SnO 2 via Electron Transfer from Graphene Quantum Dots for E ffi cient Perovskite Solar Cells, , DOI:10.1021/acsnano.7b04070.
75 V. A. Online, S. Suragtkhuu, O. Tserendavag, U. Vandandoo, A. S. R. Bati, M. Bat-erdene, J. G. Shapter, M. Batmunkh and S. Davaasambuu, E ffi ciency and stability enhancement of perovskite solar cells using reduced graphene oxide derived, 2020, 9133–9139.
76 L. L. Jiang, Z. K. Wang, M. Li, C. H. Li, P. F. Fang and L. S. Liao, Flower-like MoS 2 nanocrystals: A powerful sorbent of Li + in the Spiro-OMeTAD layer for highly efficient and stable perovskite solar cells, *J. Mater. Chem. A*, 2019, **7**, 3655–3663.
77 A. Capasso, F. Matteocci, L. Najafi, M. Prato, J. Buha, L. Cinà, V. Pellegrini, A. Di Carlo and F. Bonaccorso, Few-Layer MoS2 Flakes as Active Buffer Layer for Stable Perovskite Solar Cells, *Adv. Energy Mater.*, 2016, **6**, 1–12.
78 I. Celik, B. E. Mason, A. B. Phillips, M. J. Heben and D. Apul, Environmental Impacts from Photovoltaic Solar Cells Made with Single Walled Carbon Nanotubes, *Environ. Sci. Technol.*, 2017, **51**, 4722–4732.

1